

Article

Prediction of Mechanical Behaviours of FRP-Confined Circular Concrete Columns Using Artificial Neural Network and Support Vector Regression: Modelling and Performance Evaluation

Pang Chen ¹, Hui Wang ¹, Shaojun Cao ^{1,*} and Xueyuan Lv ²

¹ School of Civil and Transportation Engineering, Hebei University of Technology, Tianjin 300401, China; 2020029@hebut.edu.cn (P.C.); 202031603007@stu.hebut.edu.cn (H.W.)

² China Construction First Group Construction & Development Co., Ltd., Beijing 100102, China; lvxueyuan@chinaonebuild.com

* Correspondence: 2021121@hebut.edu.cn; Tel.: +86-132-8463-2829

Abstract: The prediction and control of the mechanical behaviours of fibre-reinforced polymer (FRP)-confined circular concrete columns subjected to axial loading are directly related to the safety of the structures. One challenge in building a mechanical model is understanding the complex relationship between the main parameters affecting the phenomenon. Artificial intelligence (AI) algorithms can overcome this challenge. In this study, 298 test data points were considered for FRP-confined circular concrete columns. Six parameters, such as the diameter-to-fibre thickness ratio (D/t) and the tensile strength of the FRP (f_{frp}) were set as the input sets. The existing models were compared with the test data. In addition, artificial neural networks (ANNs) and support vector regression (SVR) were used to predict the mechanical behaviour of FRP-confined circular concrete columns. The study showed that the predictive accuracy of the compressive strength in the existing models was higher than the peak compressive strain for the high dispersion of material deformation. The predictive accuracy of the ANN and SVR was higher than that of the existing models. The ANN and SVR can predict the compressive strength and peak compressive strain of FRP-confined circular concrete columns and can be used to predict the mechanical behaviour of FRP-confined circular concrete columns.

Keywords: FRP-confined circular concrete columns; artificial neural network; support vector regression; mechanical behaviours



Citation: Chen, P.; Wang, H.; Cao, S.; Lv, X. Prediction of Mechanical Behaviours of FRP-Confined Circular Concrete Columns Using Artificial Neural Network and Support Vector Regression: Modelling and Performance Evaluation. *Materials* **2022**, *15*, 4971. <https://doi.org/10.3390/ma15144971>

Academic Editor: Angelo Marcello Tarantino

Received: 7 June 2022

Accepted: 11 July 2022

Published: 17 July 2022

Publisher's Note: MDPI stays neutral with regard to jurisdictional claims in published maps and institutional affiliations.



Copyright: © 2022 by the authors. Licensee MDPI, Basel, Switzerland. This article is an open access article distributed under the terms and conditions of the Creative Commons Attribution (CC BY) license (<https://creativecommons.org/licenses/by/4.0/>).

1. Introduction

Fibre-reinforced polymers (FRPs) are widely used in composite structures and for structural strengthening owing to their light weight, high strength, and good corrosion resistance [1–7]. As shown in Figure 1, an FRP-confined circular concrete column consists of core concrete and an external confinement of wrapped FRP. σ_c is the axial compressive stress on the FRP-confined circular concrete column; σ_f is the lateral constraint stress on the core concrete of the FRP-confined circular concrete column; and σ_{cf} is the reaction force generated by the core concrete under the FRP-confined action.

In FRP-confined circular concrete columns, the core concrete is subjected to triaxial compression under axial loading, which improves the bearing capacity and ductility of the members and subsequently reduces the section size and self-weight of the members [8–11]. In addition, external confinement by the wrapping of FRP protects the core concrete from corrosion and improves the durability of the members. Relevant research has shown that the restraining action of FRP can increase the bearing capacity and ductility of core concrete by 2–46% and 14–923%, respectively [12–15]. Therefore, studying the axial compressive mechanical behaviours of FRP-confined circular concrete columns is vital in expanding their application in engineering practices.

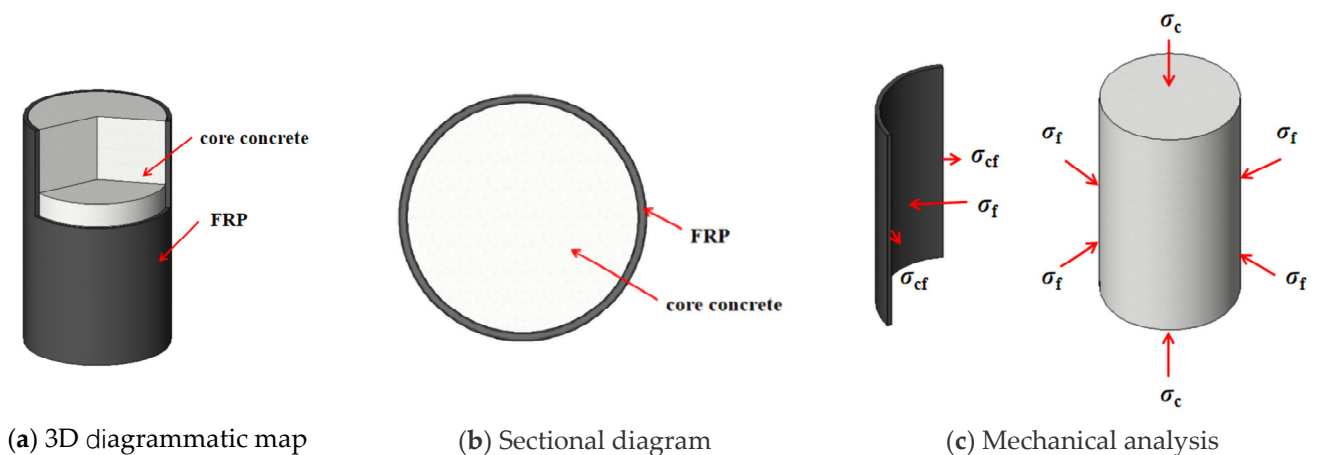


Figure 1. FRP-confined circular concrete column.

Researchers have extensively investigated the axial compressive mechanical behaviours of FRP-confined concrete columns. They have studied the influences of the diameter-to-fibre thickness ratio (D/t), the compressive strength of the core concrete (f_{co}), the strain corresponding to the compressive strength of core concrete (ϵ_{co}), the tensile strength of FRP (f_{frp}), the elastic modulus of FRP (E_{frp}), and the ultimate tensile strain of FRP (ϵ_{frp}) on the axial compressive mechanical behaviours of FRP-confined circular concrete columns and proposed their axial compression constitutive models. Fardis studied the influences of the section size and compressive strength of core concrete on the axial compressive mechanical behaviours of FRP-confined circular concrete columns and proposed a corresponding axial compression constitutive model based on the test results [16]. Saadatmanesh established an axial compression constitutive model of CFRP- and GFRP-confined circular concrete columns based on the steel-confined concrete model proposed by Mander [17,18]. Nanni studied the influence of the FRP type on the axial compressive mechanical behaviours of FRP-confined circular concrete columns and proposed their hyperbolic constitutive model based on the test results [19]. Samaan studied the influence of FRP layers on the axial compressive mechanical behaviours of GFRP-confined circular concrete columns and proposed an axial compression constitutive model [20]. Lam and Teng proposed a two-stage constitutive model of FRP-confined circular concrete columns based on experimental data, which combined a parabola and a straight line [21–24]. Chastre and Silva studied the influences of the diameter-to-fibre thickness ratio, the elastic modulus of FRP, and the strength of core concrete on the axial compressive mechanical behaviours of GFRP-confined circular concrete columns and proposed an axial compression constitutive model of FRP-confined circular concrete columns based on the test results [25]. In order to reduce the error increase in the FRP constraint model due to FRP failure, Gian proposed an effective strain analysis model of FRP-confined cylinder concrete columns based on a theoretical analysis and the test data [26]. Wu and Wei studied the effects of the ultimate tensile strain of FRP and the strength of core concrete on the axial compressive mechanical behaviours of FRP-confined circular concrete columns and proposed an axial compression constitutive model of FRP-confined circular concrete columns based on the test results [27]. With the depth of research on FRP-confined concrete columns increasing, researchers have carried out a series of research works on FRP-confined non-circular concrete columns. Gian established a simplified model of FRP-confined circular concrete columns based on the iterative constraint model proposed by himself [28]. Jiang studied the effect of FRP restraint on reducing the strength degradation of square concrete columns based on a test under the eccentric loading of FRP-confined square concrete columns [29]. He reviewed the research status of FRP-confined non-circular concrete columns with modified shapes and proved the advantage of the curving section through the influence of key parameters on the FRP constraints [30]. All the existing models are semi-empirical and semi-theoretical formulations

based on limited data, which do not consider the influence of all the parameters on the compressive strength and ultimate compressive strain of the FRP-confined circular concrete columns. The accuracy of the prediction needs to be evaluated; therefore, it is urgent to propose a reliable model that can accurately predict the axial compressive constitutive relationship of FRP-confined circular concrete columns.

In recent years, machine learning has shown unique advantages in solving various problems in structural engineering. A variety of machine learning methods have been widely applied in performance prediction, data classification, image recognition, structural simulation, etc. In particular, artificial neural networks (ANNs) and support vector regression have attracted the most attention [31–38].

ANNs are mathematical models that simulate the neural frame of a human to process complex information. They are widely used for data prediction [39,40]. Liu used an ANN and a swarm intelligence algorithm to predict the carbonation depth of recycled concrete through nine parameters, including temperature, recycled aggregate replacement rate, water absorption, and exposure time, and the results showed that the ANN performed better than the conventional formula [41]. Amiri used an ANN to predict the mechanical behaviours and durability of concrete containing constructional waste through the water-binder ratio, the recycled aggregate replacement rate, and other parameters. The results proved that the ANN had excellent accuracy in predicting the target value [42]. Jayasinghe established a shear test database of concrete beams without shear reinforcement and evaluated the forecast accuracy of the ANN and existing models. The results showed that the ANN was more accurate and is an effective tool for the influence analysis of a single parameter [43].

Support vector regression (SVR) is a regression model developed by Vapnik [44], who introduced insensitive loss functions into the support vector machine (SVM) based on statistical learning theory. It has better predictive ability. Ahmad used SVR, NMR (nuclear magnetic resonance), and an ANN to predict the splicing strength of reinforced concrete members based on the diameter of the rebar, the compressive strength of concrete, and the protective cover thickness. The results show that SVR has the highest forecasting accuracy [31]. Tran used SVR to predict the adhesion strength of the interface between FRP and concrete using the water–cement ratio, the recycled aggregate replacement rate, the sand rate, and other parameters. The results showed that SVR had good predictive performance [45].

ANNs and SVR have been successfully applied in the field of architecture and achieved ideal results [46–50]. Whether they can accurately predict the axial compressive mechanical behaviour of FRP-confined circular concrete columns needs to be evaluated. Based on this, our study collected the test data of the axial compressive mechanical behaviours of FRP-confined circular concrete columns from the relevant published literature and established a reliable database containing 298 datasets. D/t , f_{co} , ε_{co} , f_{frp} , E_{frp} , and ε_{frp} were set as input sets. Based on the established database, the forecast accuracy of the existing axial compression constitutive model for FRP-confined circular concrete columns was evaluated and analysed. ANN and SVR models were developed, and the forecast accuracy of the axial compressive mechanical behaviours of the FRP-confined circular concrete columns was evaluated and analysed using the ANN, SVR, and the existing axial compression constitutive models. Finally, based on the intelligent algorithm model, the affecting key factors were analysed using expanded parameters. Finally, the key factors affecting the axial compressive mechanical behaviours of the FRP-confined circular concrete columns were analysed based on an intelligent algorithm.

2. Database

The database relied on 298 specimens of tested data obtained from 13 studies [1,8,43–45,51–58]. The data information has been listed in Appendix A. It is crucial to collect appropriate parameters to study the axial compressive mechanical behaviour of FRP-confined circular concrete columns. Thus, such a database considers the influence of six parameters on the mechanical behaviour of

FRP-confined circular concrete columns and the influence of $D/t, f_{co}, \epsilon_{co}, f_{frp}, E_{frp}$, and ϵ_{frp} on the axial mechanical behaviour of FRP-confined circular concrete columns. Detailed information on the main parameters is presented in Table 1.

The range of the $D/t, f_{co}, \epsilon_{co}, f_{frp}, E_{frp}$, and ϵ_{frp} are shown in Figures 2 and 3. The D/t was mainly distributed in the range of 0–500. The minimum f_{co} was 9.9 MPa, the highest was 136.3 MPa, and the data between 50 MPa and 100 MPa were the highest. The ϵ_{co} was concentrated in the range of 1500–3000 $\mu\epsilon$. The f_{frp} in the range of 2000 MPa–4000 MPa was up to 65%. Most data on the E_{frp} were distributed in the range of 200–300 GPa. The data points of the ϵ_{frp} in the range of 4.5×10^4 – $5 \times 10^4 \mu\epsilon$ were the least, and maximum data points were in the range of 3×10^4 – $4.5 \times 10^4 \mu\epsilon$.

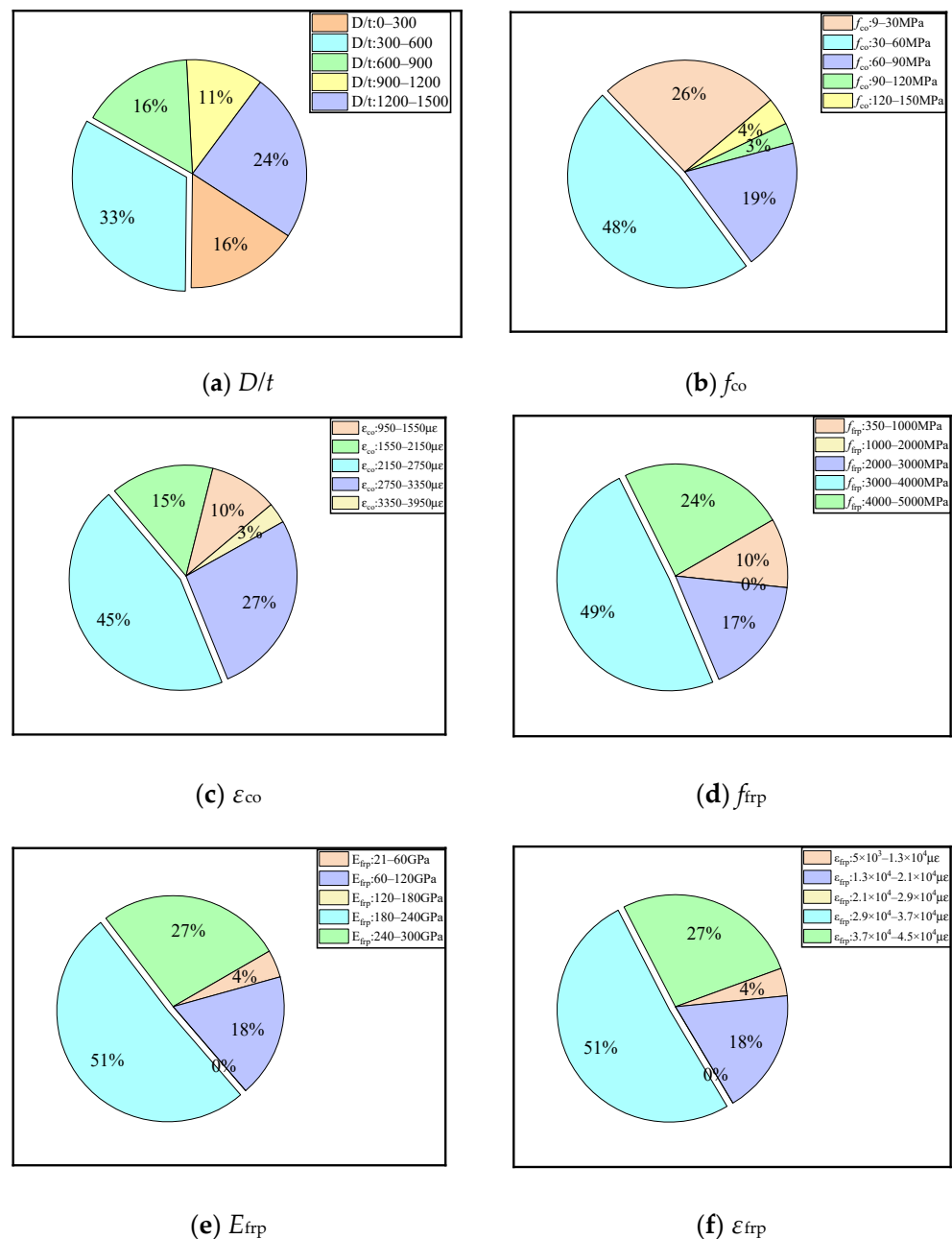


Figure 2. The value range of each parameter.

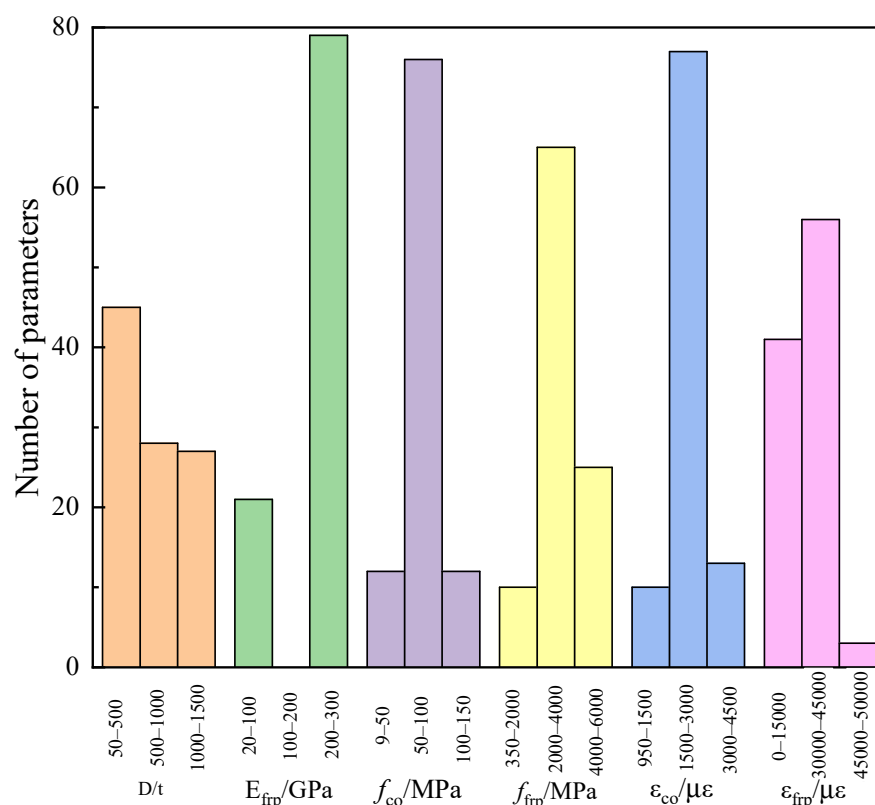


Figure 3. The histogram of each parameter distribution.

Table 1. The detailed information of main parameters.

Parameter	D/t	f_{co}/MPa	$\epsilon_{co}/\mu\epsilon$	f_{frp}/MPa	E_{frp}/GPa	$\epsilon_{frp}/\mu\epsilon$
Minimum	57.3	9.9	950	383	21.6	7200
Median	615.4	39.4	2600	3500	234	16,000
Maximum	1500.0	136.3	3850	4933	245	43,000
Average	721.2	46.7	2440	3321	196.6	16,686
Standard deviation	433.1	25.6	598	1066	71.2	4967
Skewness	0.3	1.7	-0.9	-1.1	-1.3	3.9

3. Predictive Models of the Axial Compressive Mechanical Behaviours of FRP-Confined Circular Concrete Columns

3.1. Evaluation Indices

To evaluate the predictive accuracy of the models of the axial compressive mechanical behaviours of the FRP-confined circular concrete columns, the regression coefficient (R^2), the mean square error (MSE), the mean absolute percentage error ($MAPE$), and the integral absolute error (IAE) were used to evaluate the predictive accuracy of the models. R^2 reflects the correlation between the independent and dependent variables. The closer R^2 is to 1, the higher is the correlation between the predictive value and the actual value. The MSE reflects the average error. The lower the MSE , the smaller the error between the predictive value and the actual value. $MAPE$ reflects the degree of data dispersion. The smaller the $MAPE$, the more the predictive value converges to the actual value. Additionally, the IAE reflects the predictive accuracy. The smaller the IAE , the higher the predictive accuracy of the data. All the indices

are often used to evaluate the predictive accuracy of the neural network model [42,59–62]. The design formulae for each index are given in Equations (1)–(4).

$$R^2 = \frac{(\sum_{i=1}^n (O_i - \bar{O}_i)(C_i - \bar{C}_i))^2}{\sum_{i=1}^n (O_i - \bar{O}_i)^2 \sum_{i=1}^n (C_i - \bar{C}_i)^2} \quad (1)$$

$$MSE = \frac{1}{n} \sum_{i=1}^n (C_i - O_i)^2 \quad (2)$$

$$MAPE = \frac{1}{n} \sum_{i=1}^n \left| \frac{C_i - O_i}{C_i} \right| \quad (3)$$

$$IAE = \frac{\sqrt{\sum_{i=1}^n (O_i - C_i)^2}}{\sum_{i=1}^n C_i} \times 100\% \quad (4)$$

where O_i is the actual value of the compressive strength or ultimate compressive strain (MPa/ $\mu\epsilon$); C_i is the predictive value of the compressive strength or ultimate compressive strain (MPa/ $\mu\epsilon$); \bar{O}_i is the average value of the actual value of the compressive strength or ultimate compressive strain (MPa/ $\mu\epsilon$); \bar{C}_i is the average value of the predictive value of the compressive strength or ultimate compressive strain; and n is the number of data points.

3.2. Evaluation of Existing Axial Compression Constitutive Models

3.2.1. Existing Axial Compression Constitutive Models

At present, there is much research on the axial compressive mechanical behaviour of FRP-confined circular concrete columns. The influence of key parameters on the axial compressive mechanical behaviours of FRP-confined circular concrete columns has been studied, and many axial compression constitutive models of FRP-confined circular concrete columns have been proposed. Among them, the Mander [16], Fardis [17], Lam [21], Bisby [63], Wu [64], and Youssef [65] models are widely used.

The Mander model was proposed as a steel-confined concrete model in 1988 [16] and was later adopted by the guidelines for the selection, design, and installation of FRP systems for externally strengthening concrete structures to calculate the axial compressive mechanical behaviours of FRP-confined circular concrete columns [66]. Fardis experimentally studied the axial compressive mechanical behaviours of 46 FRP-confined circular concrete columns and proposed axial compression constitutive models of CFRP-confined circular concrete columns [17]. Lam and Teng proposed a constitutive model for FRP-confined circular concrete columns combined with a parabola with a straight line [21]. Bisby studied the influence of the FRP type on the axial compressive mechanical behaviours of FRP-confined circular concrete columns and proposed a constitutive model applicable to medium and weak FRP-confined concrete columns [63]. Wu Gang proposed a simplified trilinear constitutive model for FRP-confined circular concrete columns [64]. Youssef proposed an axial compressive constitutive model of FRP-confined circular concrete columns considering the influence of the FRP type and the diameter-to-fibre thickness ratio [65]. Detailed information on each model is shown in Table 2.

Table 2. Details of existing axial compression constitutive models.

Models	Equation for Stress	Equation for Strain	Parameters	Range of Application
Mander [16]	$\frac{f_{cc}}{f_{co}} = 2.254 \sqrt{1 + \frac{7.94f_l}{f_{co}}} - \frac{2f_l}{f_{co}} - 1.254$	$\frac{\epsilon_{cc}}{\epsilon_{co}} = 5 \frac{f_{cc}}{f_{co}} - 4$	f_{co}/t_{frp} /styles of FRP	CFRP/GFRP-confined concrete columns
Fardis [17]	$\frac{f_{cc}}{f_{co}} = 1 + 4.1 \frac{f_{frp}^4}{Rf_{co}}$	$\epsilon_{cc} = 0.002 + 0.0005 \frac{E_{frp}^4}{Rf_{co}}$	R /styles of FRP	CFRP-confined circular concrete columns
Lam [21]	$\frac{f_{cc}}{f_{co}} = 1 + 2 \frac{f_l}{f_{co}}$	$\frac{\epsilon_{cc}}{\epsilon_{co}} = 15 \frac{f_l}{f_{co}} + 2$	f_{co}/t_{frp} /styles of FRP/ f_{frp}	CFRP/GFRP-confined circular concrete columns
Bisby [63]	$\frac{f_{cc}}{f_{co}} = 1 + 3.587f_r^{0.84}$	$\frac{\epsilon_{cc}}{\epsilon_{co}} = 1 + 0.024 \frac{f_r}{f_{co}}$	styles of FRP	Medium and weak FRP-confined concrete column
Wu [64]	$\frac{f_{cc}}{f_{co}} = 1.316 + 2.098 \frac{f_l}{f_{co}} - 0.317 \left(\frac{f_l}{f_{co}}\right)^2$	$\epsilon_{cc} = 3.223\epsilon_{frp} \left(\frac{f_l}{f_{co}}\right)^{0.44}$	f_{co}/t_{frp} /styles of FRP/ R	AFRP/CFRP/GFRP-confined circular concrete columns
Youssef [65]	$\frac{f_{cc}}{f_{co}} = 1 + 2.25f_r^{1.25}$	$\epsilon_{cc} = 0.003368 + 0.259 \frac{f_r}{f_{co}} \left(\frac{f_{frp}}{E_{frp}}\right)^{0.5}$	t_{frp} /styles of FRP/ R	CFRP/GFRP-confined circular concrete columns

Note: f_{cc} : compressive strength of FRP-confined circular concrete columns (MPa); f_{co} : compressive strength of core concrete (MPa); ϵ_{cc} : strain corresponding to compressive strength of FRP-confined circular concrete columns ($\mu\epsilon$); ϵ_{co} : strain corresponding to compressive strength of core concrete ($\mu\epsilon$); f_{frp} : tensile strength of FRP (MPa); E_{frp} : elastic modulus of FRP (GPa); R : section radius of specimen (mm); f_r : effective lateral constraint stress provided by FRP (MPa); f_l : lateral constraint stress provided by FRP (MPa).

3.2.2. Predictive Results of Existing Axial Compression Constitutive Models

Based on the established database, the predictive accuracies of the six axial compressive constitutive models of FRP-confined circular concrete columns were compared and analysed. The results of the compressive strength of each model are shown in Figure 4.

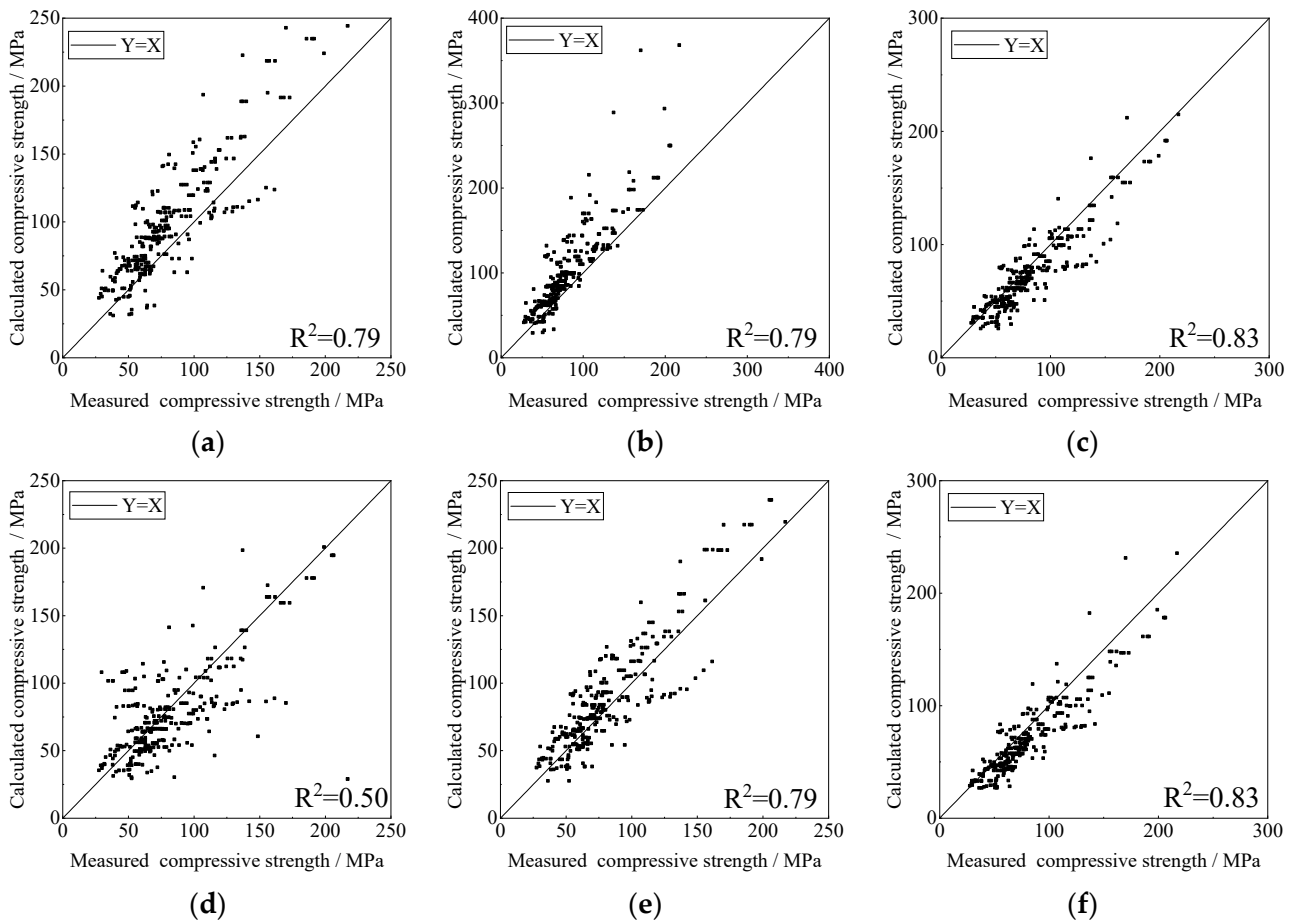


Figure 4. Predictive results of compressive strength. (a) Mander Model, (b) Fardis Model, (c) Lam Model, (d) Bisby Model, (e) Wu Model, (f) Youssef Model.

As shown in the figure, most of the data points of the Mander [16] and Fardis [17] models are above a straight line, indicating that both the models overestimate the compressive strength of FRP-confined circular concrete columns. However, most of the data points of the Bisby [63] and Youssef [65] models are below the best fit line, indicating that both these models underestimate the compressive strength of FRP-confined circular concrete columns. The predictive capability of the Lam [21] and Wu [64] models is good, and the data points are uniformly distributed on both sides of the best fit line. Among them, the Lam model [21] has a more concentrated distribution of data points, and the Lam model [21] has the highest predictive accuracy of compressive strength for FRP-confined circular concrete columns.

The predictive results of the models for strain corresponding to the compressive strength of the FRP-confined circular concrete columns are shown in Figure 5. It can be observed from the figure that most of the data points of the Mander [16], Lam [21], and Wu [64] models are above the best fit line, indicating that these models overestimate the peak compressive strain of FRP-confined circular concrete columns. Most of the data points of the Fardis [17], Bisby [63], and Youssef [65] models are below the best fit line. This indicates that these models underestimated the peak compressive strain of FRP-confined circular concrete columns. The distribution of the data points in each figure is scattered, indicating that the predictive accuracy of the peak compressive strain in the existing axial compressive constitutive models of FRP-confined circular concrete columns is poor.

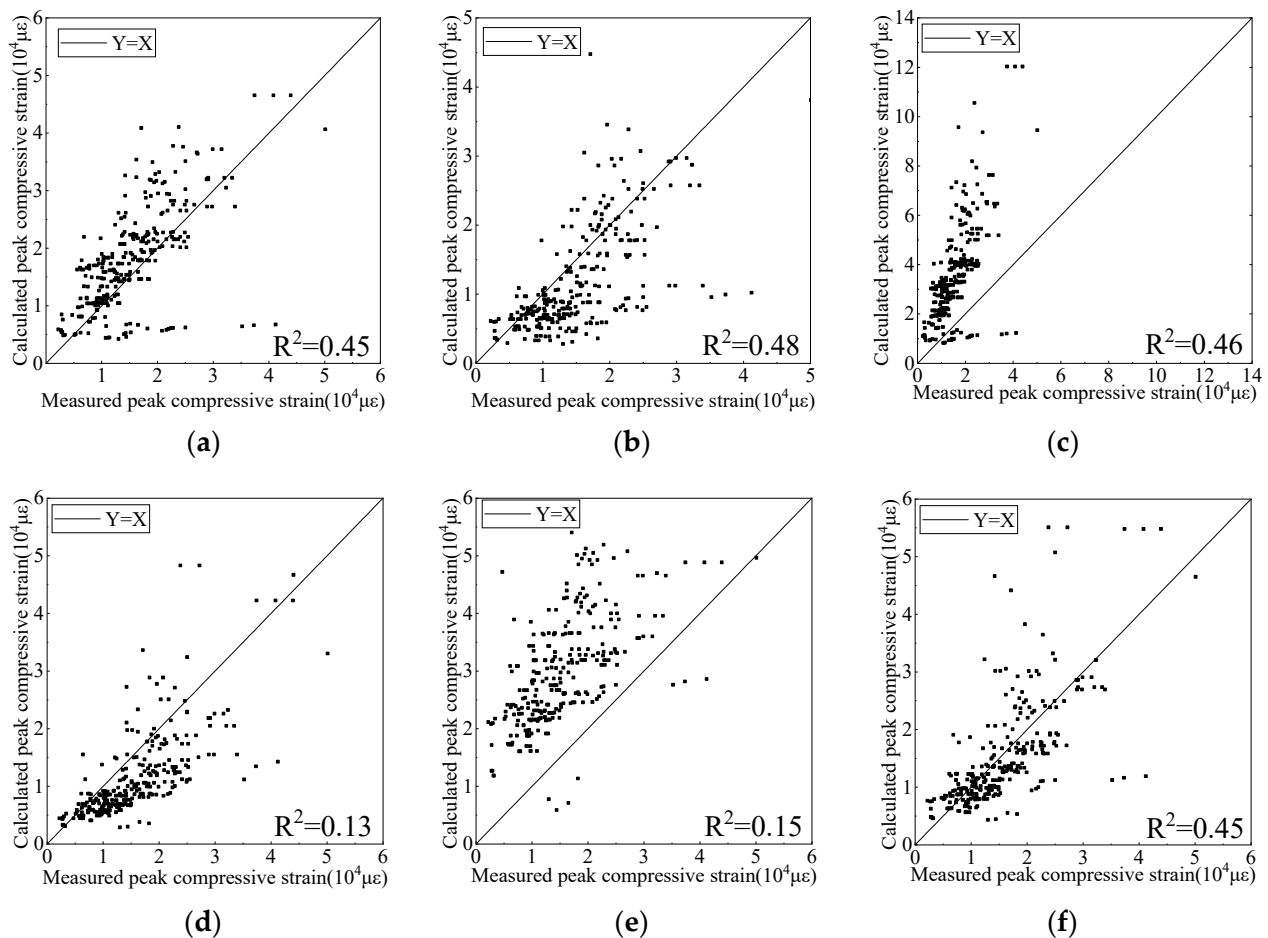


Figure 5. Predictive results of peak compressive strain. (a) Mander Model, (b) Fardis Model, (c) Lam Model, (d) Bisby Model, (e) Wu Model, (f) Youssef Model.

The evaluation indexes (R^2 , MSE , $MAPE$, and IAE) for the predictive accuracy of the compressive strength of the above models are listed in Table 3. It can be seen from Table 3

that the predictive accuracy of all the models is good, and the R^2 is above 0.5. The Lam model [21] had the highest predictive accuracy, with an R^2 of up to 0.83 and the lowest average error and a small dispersion.

Table 3. Predictive accuracy of compressive strength.

Models	R^2	MSE	MAPE	IAE/%
Mander [16]	0.79	788.5	0.22	1.64
Fardis [17]	0.79	1078.3	0.21	1.86
Lam [21]	0.83	271.9	0.20	1.30
Bisby [63]	0.50	707.5	0.27	1.99
Wu [64]	0.79	393.5	0.19	1.31
Youssef [65]	0.83	317.8	0.22	1.45

Table 4 summarises the evaluation indices (R^2 , MSE, MAPE, and IAE) of the predictive accuracy in the peak compressive strain of all the models. It can be observed from Table 4 that the predictive accuracy of the peak compressive strain is lower than that of the compressive strength for all the models. The regression coefficient of the Fardis model [17] with the highest predictive accuracy was only 0.48; it had a high dispersion and error.

Table 4. Predictive accuracy of peak compressive strain.

Models	R^2	MSE/10 ⁷	MAPE	IAE/%
Mander [16]	0.45	5.45	0.39	2.36
Fardis [17]	0.48	5.69	0.61	3.48
Lam [21]	0.46	63.49	0.59	4.15
Bisby [63]	0.13	9.18	0.79	4.86
Wu [64]	0.15	47.10	0.52	3.97
Youssef [65]	0.45	5.49	0.33	2.81

3.3. Evaluation of Predictive Models Based on ANN and SVR

The predictive accuracy of the compressive strength and peak compressive strain by the existing axial compressive constitutive model of FRP-confined circular concrete columns is low and that of the peak compressive strain is especially poor. Therefore, a new predictive model is urgently required to predict the axial compressive mechanical behaviour of FRP-confined circular concrete columns.

3.3.1. Machine Learning Models Artificial Neural Networks (ANNs)

An ANN is an information processing system that simulates the structural and functional characteristics of a biological neural system [61]. It includes input, hidden, and output layers. Each of these layers contains some nodes, which are interconnected to the elements in the subsequent layers [67]. The accuracy and the precision of the ANN is highly dependent on the structure of the developed models as well as the model parameters. These parameters contain the number of nodes in the hidden layers, the momentum rate, the learning cycle, and the learning accuracy. The basic idea is that in each hidden layer node, the weighted inputs from the previous layer are added together and the deviation is added to the system, where the weight depends on the momentum rate, and the deviation depends on the learning accuracy. This combination is then passed through a nonlinear activation function to form the output of each hidden neuron [68]. The back-propagation algorithm is often used to train ANN. Training is defined as the procedure for finding the optimal weights of the network so that the prediction error is minimized. In the learning

cycle, the results are back-propagated, and the weights and the bias are adjusted in such a way that the obtained error is minimized [69].

A MATLAB-based program with a graphical user interface (GUI) was developed to train and evaluate the ANN model. The ANN model divided the established database into two parts: 80% for training (general is 70–90%) and 20% for testing (general is 10–30%). According to the predictive target, there are six and one nodes in the input and output layers, respectively; the momentum rate is 0.5; the learning cycle is 10^3 ; and the learning accuracy is 4×10^{-7} .

The number of nodes in the hidden layer plays a vital role in the predictive accuracy of an ANN. To determine this, the predictive accuracies of different numbers of nodes in the hidden layers were compared and analysed. The influence of the number of nodes in the hidden layers on the predictive accuracy of the compressive strength is shown in Figure 6, and the influence of the number of nodes in the hidden layers on the predictive accuracy of peak compressive strain is shown in Figure 7. It can be seen that when the number of nodes in the hidden layers is 10, the *MSE* of the compressive strength and peak compressive strain is the lowest, and R^2 is the highest. The predictive accuracy of the ANN model was the highest. Therefore, when predicting the compressive strength and peak compressive strain, the number of nodes in the hidden layers in the ANN model was 10.

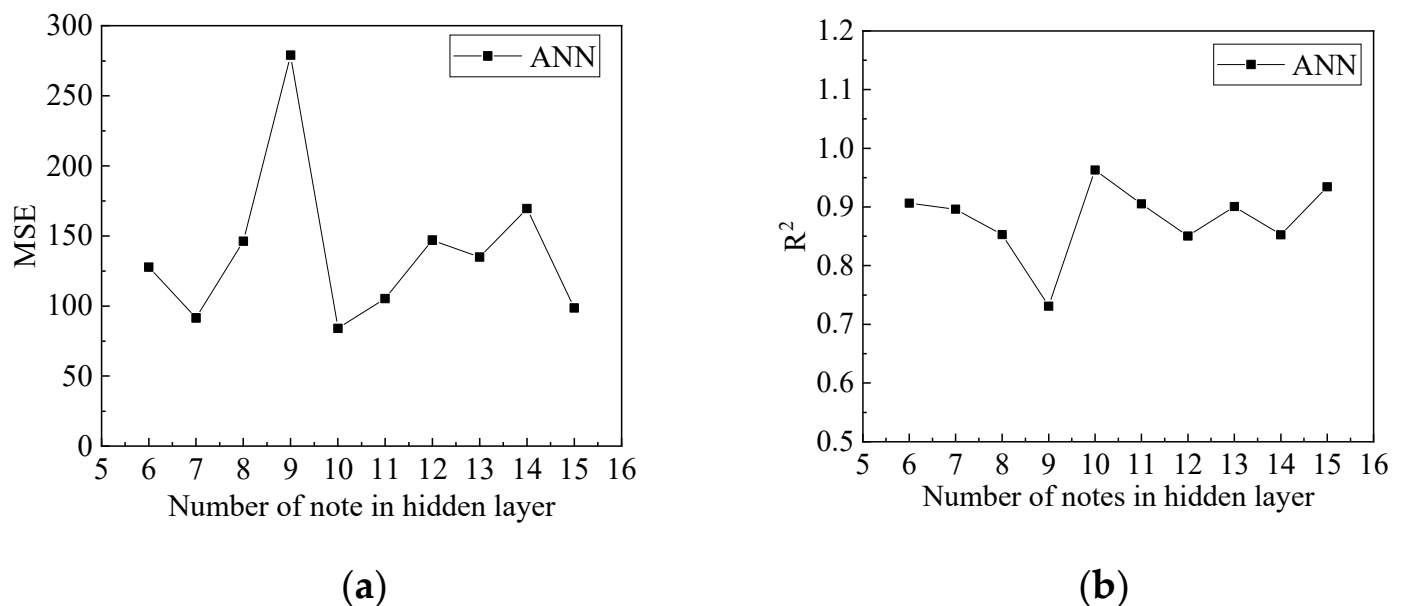


Figure 6. Influence of changes in the number of hidden layers on predictive accuracy of compressive strength: (a) the influence of changes in the number of hidden layers on *MSE*; (b) the influence of changes in the number of hidden layers on R^2 .

Support Vector Regression (SVR)

The SVM is an intelligent algorithm for general classification problems, first proposed by Boser in 1992 [70]. Unlike traditional neural networks based on empirical risk minimisation, SVR is based on the principle of structural risk minimisation, which aims to minimise the upper bound of the expected risk and avoids reliance on the designer's empirical knowledge. Vapnik introduced an insensitive loss function into the SVM to form a support vector regression (SVR) [44].

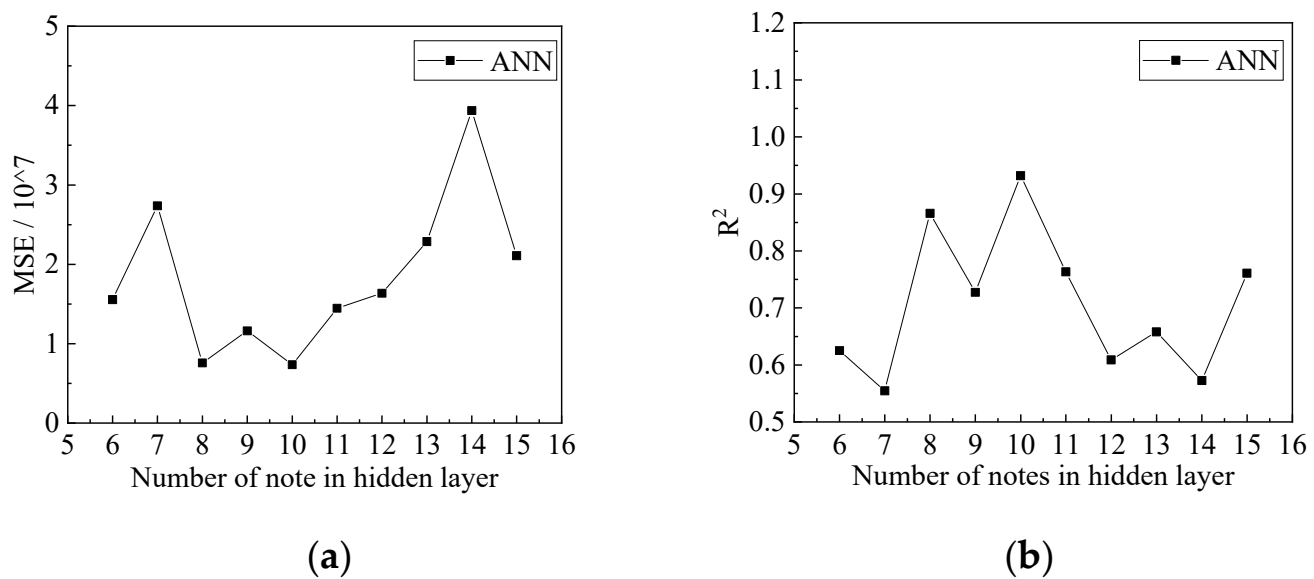


Figure 7. Influence of changes in the number of hidden layers on predictive accuracy of peak compressive strain: (a) The influence of changes in the number of hidden layers on MSE; (b) the influence of changes in the number of hidden layers on R^2 .

For the SVR model, the established database was divided into two parts: 80% for training and 20% for testing. The SVR model involves three parameters: ϵ (insensitive loss function), C (regularised constant), and g (kernel coefficient). In SVR, the main goal is to obtain a function that differs at most ϵ from the actual targets for all training data, while being as flat as possible [71]. The smaller the ϵ , the smaller the error of the regression function and the higher the degree of model fitting, where C is the regularized constant specified by the user. It is defined as the penalty factor to indicate the trade-off between the flatness of the function and the empirical error. C was mainly used to prevent overfitting. The higher the C , the more the samples with a training error greater than ϵ are punished, and the stronger is the predictive ability [72]. g is the kernel coefficient. The choice of kernel function is closely related to the performance of the SVR. The commonly used kernel functions in the regression include the linear kernel function, the polynomial kernel function, the radial basis function (RBF), and the sigmoid kernel function. Considering the infinite dimensional feature space corresponding to the RBF, the RBF is adopted in this study. Its expression is shown in Equation (5).

$$K(x_i, x_j) = e^{-g\|x_i - x_j\|^2} \quad (5)$$

where x_i, x_j is the input vector, and g is the key parameter of the RBF which can affect the smoothness of the function. The larger the g , the better the predictive effect of the training set.

To determine the optimal values of ϵ , C , and g in the SVR, each value is tested in a certain space on the premise of specifying the step. Then, based on the flow of the SVR algorithm, the parameter values of the SVR with optimal accuracy are derived: $\epsilon = 0.01$, $C = 20$, and $g = 0.3$. The flow of the SVR algorithm is illustrated in Figure 8.

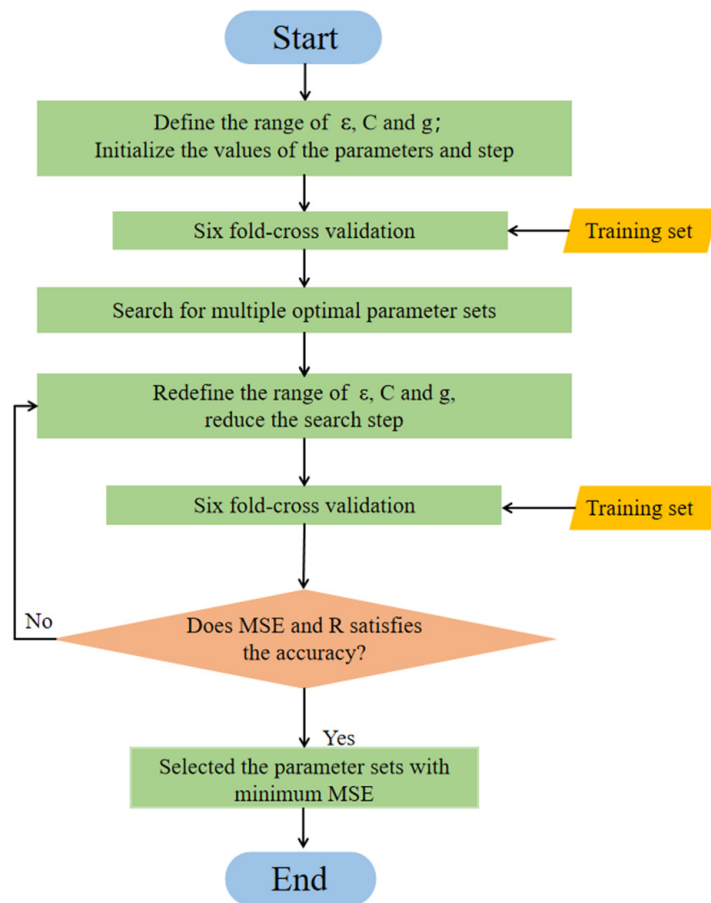


Figure 8. The SVR algorithm flow.

3.3.2. Predictive Results and Discussion of ANN and SVR

Based on the established database, the comparison between the ANN and SVR models for the predictive results of compressive strength and peak compressive strain are shown in Figures 9–12, respectively. It can be seen from Figures 9–12 that the ANN and SVR models can accurately predict the compressive strength and peak compressive strain of FRP-confined circular concrete columns, and the predictive accuracy is much higher than that of their existing axial compressive constitutive models.

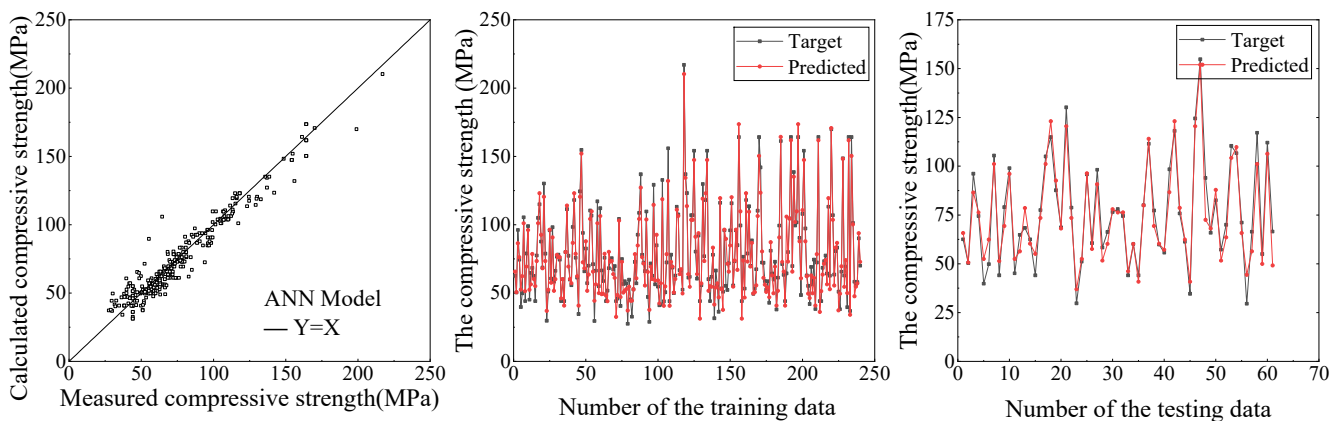


Figure 9. Predictive results of compressive strength by ANN.

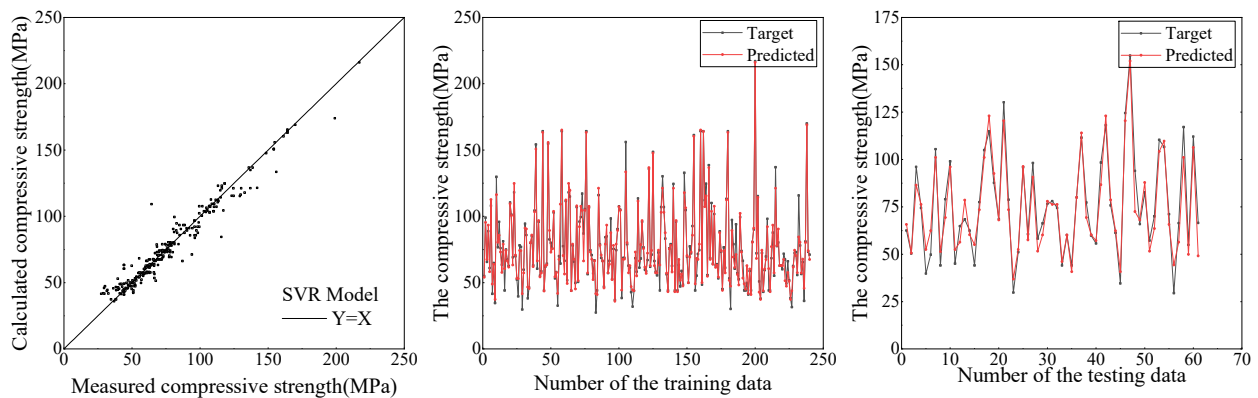


Figure 10. Predictive results of compressive strength by SVR.

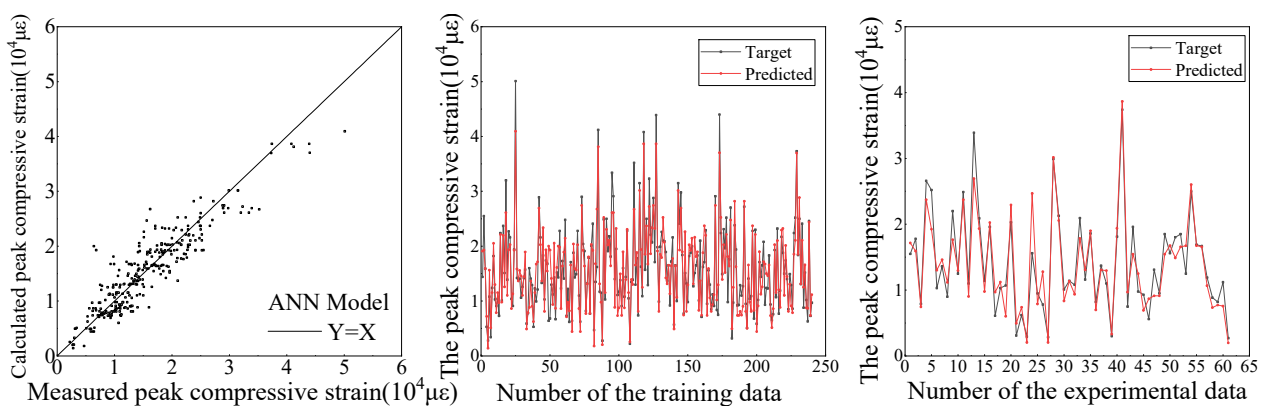


Figure 11. Predictive results of peak compressive strain by ANN.

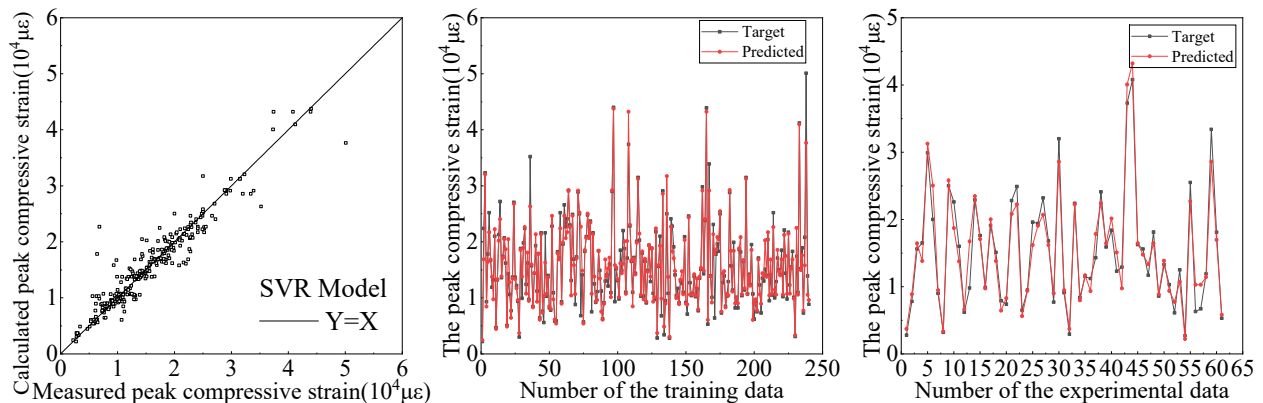


Figure 12. Predictive results of peak compressive strain by SVR.

Among the existing axial compressive constitutive models for FRP-confined circular concrete columns, the Lam [21] and Fardis [17] models have the highest predictive accuracies for the compressive strength and peak compressive strain of FRP-confined circular concrete columns, respectively. The evaluation indexes of the predictive accuracy for the ANN, SVR, Lam [21], and Fardis [17] models are listed in Table 5. It can be seen that the predictive accuracy of the SVR model for the compressive strength and peak compressive strain of FRP-confined circular concrete columns is slightly higher than that of the ANN model and far higher than that of the Lam [21] and Fardis [17] models. In the SVR model, the R^2 of the compressive strength and peak compressive strain is up to 0.96 and 0.94, respectively. In conclusion, the SVR model proposed in this study can provide an approxi-

mate basis for revising and unifying the compressive strength and peak compressive strain formulas for FRP-confined circular concrete columns.

Table 5. Predictive accuracy analysis of compressive strength and peak compressive strain.

Performance Indices	Compressive Strength			Peak Compressive Strain		
	ANN	SVR	Lam [21]	ANN	SVR	Fardis [17]
R^2	0.92	0.96	0.83	0.87	0.94	0.48
MAPE	0.11	0.09	0.20	0.18	0.13	0.61
IAE/%	0.09	0.07	1.30	0.15	0.11	3.48
MSE	84.00	63.46	271.9	0.74×10^7	0.47×10^7	5.69×10^7

4. Parameter Analysis

An ANN was used to accurately analyse the influence of D/t , f_{co} , f_{frp} , E_{frp} , f_{cc}/f_{co} , and $\varepsilon_{cc}/\varepsilon_{co}$ on the axial compressive mechanical behaviour of FRP-confined circular concrete columns. While analysing the influence of each parameter, the values of the other parameters were set as the average value of each parameter in the established database.

The influence of D/t on the compressive strength and peak compressive strain of the FRP-confined circular concrete columns is shown in Figure 13. It can be seen that both the compressive strength and the peak compressive strain of FRP-confined circular concrete columns decrease with an increase in the D/t of the specimen. When the D/t increased from 200 to 1000, the compressive strength decreased from 130 MPa to 60 MPa and the peak compressive strain decreased from 3×10^4 to 10^4 . When the D/t increases and the section size of the core concrete remains unchanged, the fibre thickness decreases and the force of constraint it can provide decreases, thus reducing the bearing capacity and ductility of the specimens [73–77].

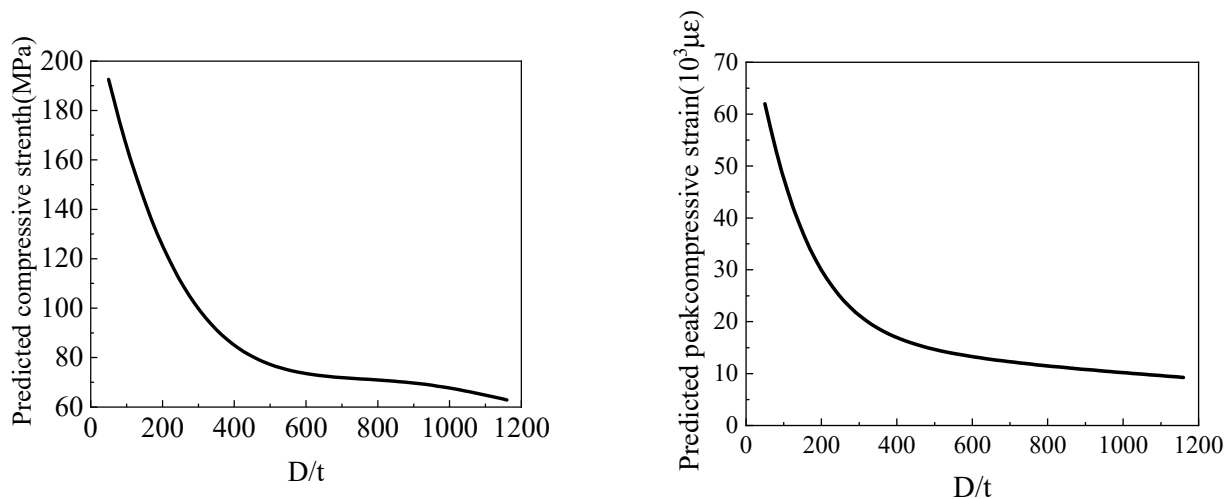


Figure 13. The influence of D/t on compressive strength and peak compressive strain.

The influence of the E_{frp} on the compressive strength and peak compressive strain of the FRP-confined circular concrete columns is shown in Figure 14. It can be seen that the compressive strength of the FRP-confined circular concrete columns is positively correlated with the E_{frp} , whereas the peak compressive strain is negatively correlated with the E_{frp} . When the E_{frp} increases from 40 GPa to 200 GPa, the compressive strength increases from 90 MPa to 150 MPa, and the peak compressive strain decreases from 2.5×10^4 to 1.5×10^4 . When the E_{frp} increases, the elastic deformation resistance, the brittleness of the specimens, and the bearing capacity of the specimens increase, and the ductility decreases [12,78,79].

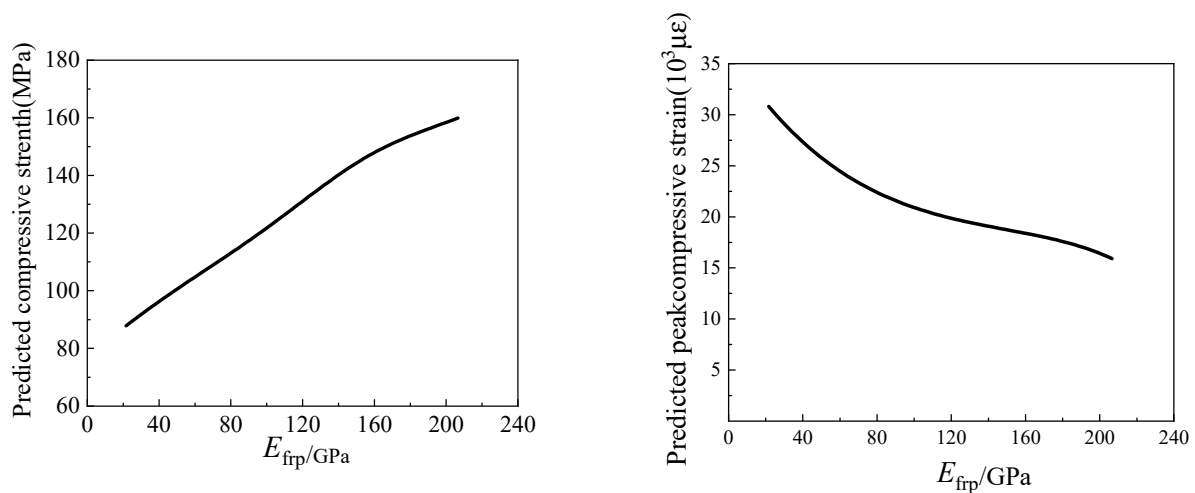


Figure 14. The influence of E_{frp} on compressive strength and peak compressive strain.

The influence of f_{frp} on the compressive strength and peak compressive strain of the FRP-confined circular concrete columns is shown in Figure 15. It can be observed that the compressive strength and the peak compressive strain of the FRP-confined circular concrete columns increase with an increase in f_{frp} . When f_{frp} increases from 800 MPa to 4000 MPa, the compressive strength increases from 50 MPa to 250 MPa, and the peak compressive strain increases from 8×10^3 to 4×10^4 . When f_{frp} increases, the force of the constraint provided by the FRP increases, and the bearing capacity and the ductility of the specimens are improved [51,80,81].

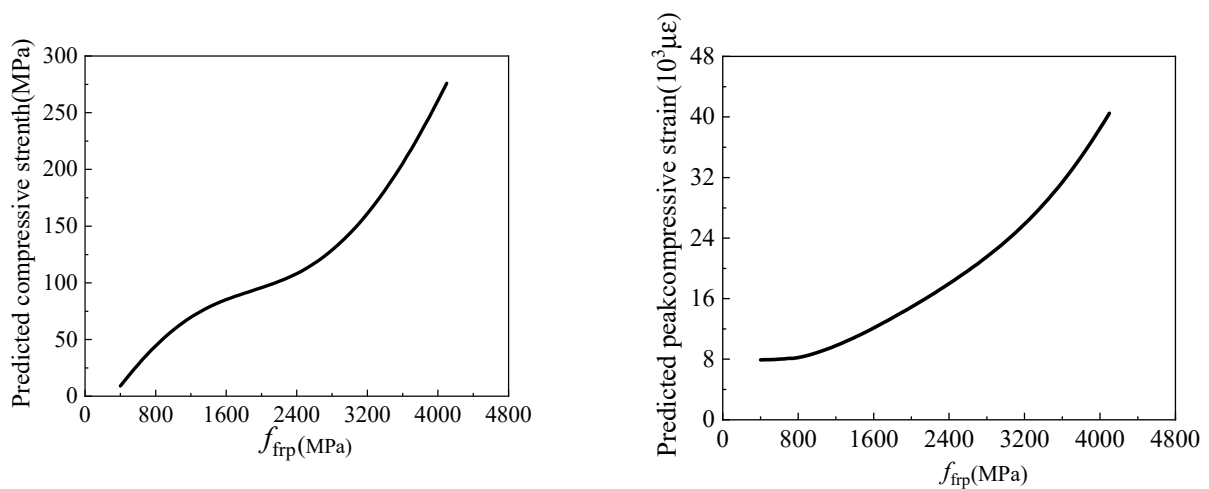


Figure 15. The influence of f_{frp} on compressive strength and peak compressive strain.

The influence of f_{co} on the compressive strength and peak compressive strain of the FRP-confined circular concrete columns is shown in Figure 16. It can be seen that the compressive strength of the FRP-confined circular concrete columns is positively correlated with f_{co} , while the peak compressive strain of the FRP-confined circular concrete columns is negatively correlated with f_{co} . When f_{co} increases from 40 MPa to 100 MPa, the compressive strength of the FRP-confined circular concrete columns increases from 90 MPa to 160 MPa, and their peak compressive strain drops from 1.6×10^4 to 4×10^3 . When f_{co} increased, the overall strength, brittleness, and the bearing capacity of the specimens increased, and the ductility decreased [82–84].

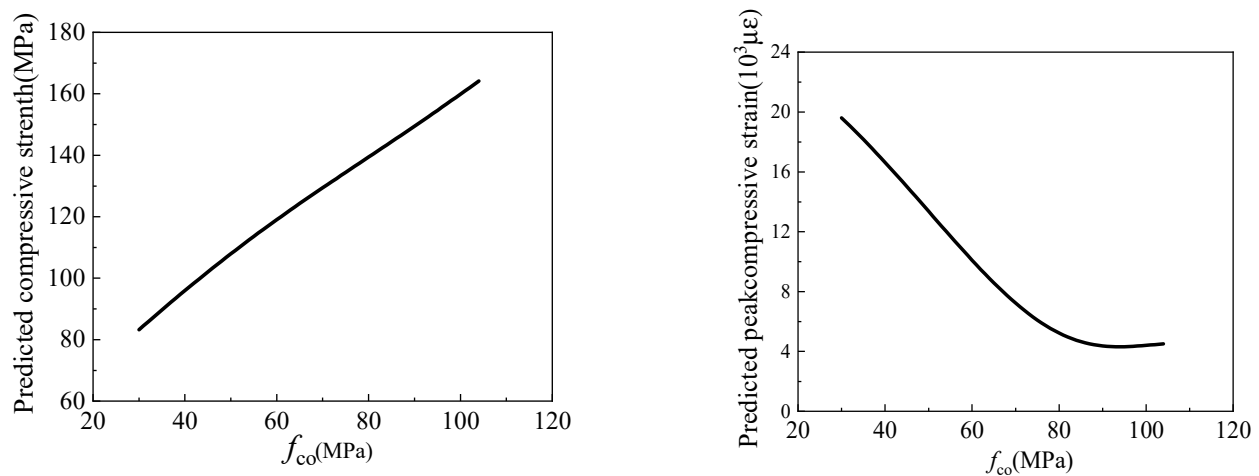


Figure 16. The influence of f_{co} on compressive strength and peak compressive strain.

The influence of the mechanical behaviours of the core concrete on the FRP-confined circular concrete columns is shown in Figure 17. It can be seen that f_{cc}/f_{co} is negatively correlated with f_{co} , while $\varepsilon_{cc}/\varepsilon_{co}$ is positively correlated with ε_{co} . When f_{co} increases from 40 MPa to 100 MPa, f_{cc}/f_{co} drops from 2.5 to 1.5. When ε_{co} increases from 3000 $\mu\varepsilon$ to 6000 $\mu\varepsilon$, $\varepsilon_{cc}/\varepsilon_{co}$ increases from 4 to 5. When f_{co} increases, its ductility decreases, and the restraint of FRP on the core concrete weakens. Additionally, when ε_{co} increases, its ductility increases. The restraint effect of FRP on core concrete is strengthened.

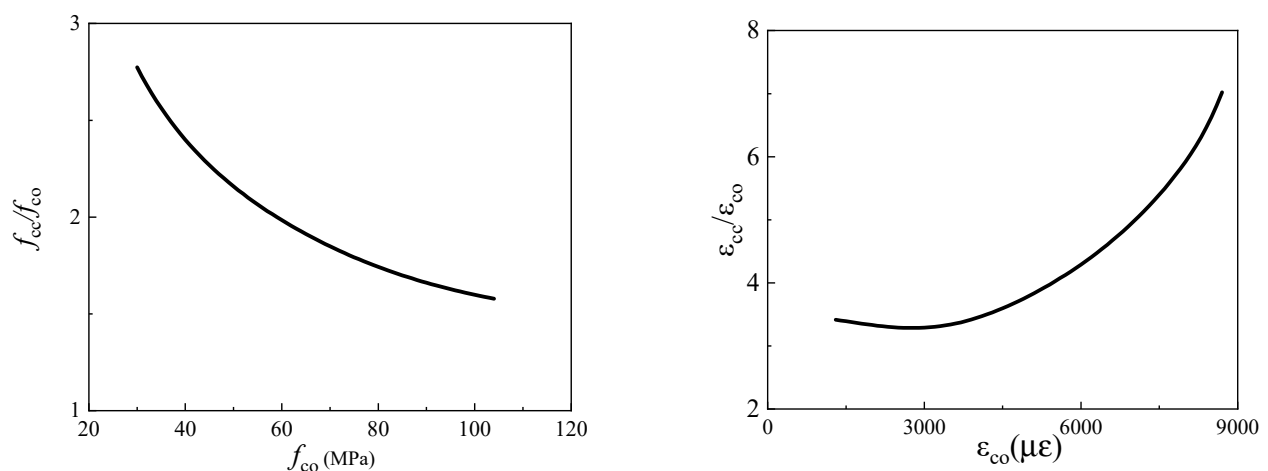


Figure 17. The influence of mechanical behaviours of core concrete on FRP-confined circular concrete columns.

5. Conclusions

This study evaluated the existing axial compressive constitutive model of FRP-confined circular concrete columns and established a predictive model for the axial compressive mechanical behaviours of FRP-confined circular concrete columns based on ANNs and SVR. The main conclusions are as follows.

- (1) A database of the axial compressive mechanical behaviours of FRP-confined circular concrete columns was established from the relevant published literature, which included 298 datasets. The effects of D/t , f_{co} , ε_{co} , f_{frp} , E_{frp} , and ε_{frp} on the axial mechanical behaviours of FRP-confined circular concrete columns were considered.
- (2) Comparing and analysing the existing axial compressive constitutive model of FRP-confined circular concrete columns, the Lam model [21] exhibited the highest predictive accuracy for the compressive strength of FRP-confined circular concrete columns.

- (3) Comparing and analysing the existing axial compressive constitutive models of FRP-confined circular concrete columns, the Fardis model [17] exhibited the highest predictive accuracy for the peak compressive strain of FRP-confined circular concrete columns.
- (4) The ANN and SVR models can be used to predict the axial mechanical behaviours of FRP-confined circular concrete columns. Their predictive accuracy was much higher than that of the existing axial compressive constitutive model of FRP-confined circular concrete columns, and SVR had the highest predictive accuracy.
- (5) An intelligent algorithm was used to analyse the parameters of the axial mechanical behaviour of FRP-confined circular concrete columns. The analysis results show that D/t is positively correlated with the compressive strength, whereas f_{co} , f_{frp} , and E_{frp} are negatively correlated with the compressive strength of the FRP-confined circular concrete columns. The f_{frp} is positively correlated with the peak compressive strain, whereas D/t , E_{frp} , and f_{co} are negatively correlated with the peak compressive strain of FRP-confined circular concrete columns.

Author Contributions: Conceptualization, S.C.; Data curation, X.L.; Formal analysis, H.W.; Project administration, P.C.; Supervision, P.C.; Validation, X.L.; Writing—original draft, H.W.; Writing—review & editing, S.C. All authors have read and agreed to the published version of the manuscript.

Funding: This research was funded by the financial support of the National Natural Science Foundation of China (Project No. 52108132), the Natural Science Foundation of Hebei Province (Project No. E2021202067), the Colleges and Universities in Hebei Province Science and Technology Research (Project No. QN2021037), and the China Construction First Bureau (Group) Co., Ltd. Technology research and development projects (Project No. KJYF-2021-26-03).

Data Availability Statement: No new data were created or analyzed in this study. Data sharing is not applicable to this article.

Conflicts of Interest: The authors declare no conflict of interest.

Appendix A

Table A1. Database information.

Reference	Parameters	Time	Number of Data
[1]	D/t , f_{co} (MPa), ε_{co} ($\mu\epsilon$), f_{frp} (MPa), E_{frp} (GPa), ε_{frp} ($\mu\epsilon$), CFRP	2012	30
[8]	D/t , f_{co} (MPa), ε_{co} ($\mu\epsilon$), f_{frp} (MPa), E_{frp} (GPa), ε_{frp} ($\mu\epsilon$), CFRP	2018	21
[43]	D/t , f_{co} (MPa), ε_{co} ($\mu\epsilon$), f_{frp} (MPa), E_{frp} (GPa), ε_{frp} ($\mu\epsilon$), CFRP, GFRP	2001	4
[44]	D/t , f_{co} (MPa), ε_{co} ($\mu\epsilon$), f_{frp} (MPa), E_{frp} (GPa), ε_{frp} ($\mu\epsilon$), CFRP, GFRP	2001	16
[45]	D/t , f_{co} (MPa), ε_{co} ($\mu\epsilon$), f_{frp} (MPa), E_{frp} (GPa), ε_{frp} ($\mu\epsilon$), CFRP	2012	12
[51]	D/t , f_{co} (MPa), ε_{co} ($\mu\epsilon$), f_{frp} (MPa), E_{frp} (GPa), ε_{frp} ($\mu\epsilon$), CFRP	2020	16
[52]	D/t , f_{co} (MPa), ε_{co} ($\mu\epsilon$), f_{frp} (MPa), E_{frp} (GPa), ε_{frp} ($\mu\epsilon$), CFRP, GFRP	2016	80
[53]	D/t , f_{co} (MPa), ε_{co} ($\mu\epsilon$), f_{frp} (MPa), E_{frp} (GPa), ε_{frp} ($\mu\epsilon$), CFRP, GFRP	2019	22
[54]	D/t , f_{co} (MPa), ε_{co} ($\mu\epsilon$), f_{frp} (MPa), E_{frp} (GPa), ε_{frp} ($\mu\epsilon$), GFRP	2018	8
[55]	D/t , f_{co} (MPa), ε_{co} ($\mu\epsilon$), f_{frp} (MPa), E_{frp} (GPa), ε_{frp} ($\mu\epsilon$), CFRP	2004	12
[56]	D/t , f_{co} (MPa), ε_{co} ($\mu\epsilon$), f_{frp} (MPa), E_{frp} (GPa), ε_{frp} ($\mu\epsilon$), CFRP	2013	17
[57]	D/t , f_{co} (MPa), ε_{co} ($\mu\epsilon$), f_{frp} (MPa), E_{frp} (GPa), ε_{frp} ($\mu\epsilon$), CFRP	2018	45
[58]	D/t , f_{co} (MPa), ε_{co} ($\mu\epsilon$), f_{frp} (MPa), E_{frp} (GPa), ε_{frp} ($\mu\epsilon$), CFRP	2010	15

References

1. Liu, T.Q. *Study on Material Properties and Mechanical Properties of CFRP Confined Concrete*; China University of Mining & Technology: Beijing, China, 2012. (In Chinese)
2. Fathalla, E.; Rajapakse, R.; Mihaylov, B.I. Modeling the shear behavior of deep beams strengthened with FRP sheets. *Eng. Struct.* **2022**, *260*, 114232. [[CrossRef](#)]
3. Zhou, Y.; Liu, X.; Xing, F.; Cui, H.; Sui, L. Axial compressive behavior of FRP-confined lightweight aggregate concrete: An experimental study and stress-strain relation model. *Constr. Build. Mater.* **2016**, *119*, 1–15. [[CrossRef](#)]
4. Omar, I.A.; ElGawady, M.A. Behavior of hollow FRP–concrete–steel columns under static cyclic axial compressive loading. *Eng. Struct.* **2016**, *123*, 77–88.
5. Fakharifar, M.; Chen, G. Compressive behavior of FRP-confined concrete-filled PVC tubular columns. *Compos. Struct.* **2016**, *141*, 91–109. [[CrossRef](#)]
6. Zhou, Y.; Li, M.; Sui, L.; Xing, F. Effect of sulfate attack on the stress–strain relationship of FRP-confined concrete. *Constr. Build. Mater.* **2016**, *110*, 235–250. [[CrossRef](#)]
7. Chen, L.; Ozbakkaloglu, T. Corner strengthening of square and rectangular concrete-filled FRP tubes. *Eng. Struct.* **2016**, *117*, 486–495. [[CrossRef](#)]
8. Shen, Y. *Compressive Properties of CFRP Confined Steel Fiber Reinforced Concrete Cylindrical Shaft*; Xian University of Architecture and Technology: Xi'an, China, 2018. (In Chinese)
9. Guo, Y.C.; Xiao, S.H.; Zeng, J.J.; Su, J.Y.; Li, T.Z.; Xie, Z.H. Behavior of concrete-filled FRP tube columns internally reinforced with FRP-steel composite bars under axial compression. *Constr. Build. Mater.* **2022**, *315*, 125714. [[CrossRef](#)]
10. Wang, W.; Sheikh, M.N.; Hadi, M.N.S.; Gao, D.; Chen, G. Behaviour of concrete-encased concrete-filled FRP tube (CCFT) columns under axial compression. *Eng. Struct.* **2017**, *147*, 256–268. [[CrossRef](#)]
11. Eid, R.; Paultre, P. Compressive behavior of FRP-confined reinforced concrete columns. *Eng. Struct.* **2017**, *132*, 518–530. [[CrossRef](#)]
12. Wu, G.; Wu, Z.S.; Lv, Z.S. Study on stress-strain relationship of FRP confined concrete cylinder with softening section. *J. Civ. Eng.* **2006**, *39*, 7–14. (In Chinese)
13. Kashi, A.; Ramezani-pour, A.A.; Moodi, F. Durability evaluation of retrofitted corroded reinforced concrete columns with FRP sheets in marine environmental conditions. *Constr. Build. Mater.* **2017**, *151*, 520–533. [[CrossRef](#)]
14. Toutanji, H.; Saafi, M. Durability studies on concrete columns encased in PVC–FRP composite tubes. *Compos. Struct.* **2001**, *54*, 27–35. [[CrossRef](#)]
15. Ahmed, A.; Guo, S.; Zhang, Z.; Shi, C.; Zhu, D. A review on durability of fiber reinforced polymer (FRP) bars reinforced seawater sea sand concrete. *Constr. Build. Mater.* **2020**, *256*, 119484. [[CrossRef](#)]
16. Mander, J.B.; Priestley, M.J.N. Theoretical stress-strain model for confined concrete. *J. Struct. Eng.* **1988**, *114*, 1804–1826.
17. Fardis, M.N.; Khalili, H. Concrete encased in fiberglass-reinforced plastic. *ACI Struct. J.* **1981**, *78*, 440–446.
18. Lam, L.; Teng, J.G.; Cheung, C.H.; Xiao, Y. FRP-confined concrete under axial cyclic compression. *Cem. Concr. Compos.* **2006**, *28*, 949–958. [[CrossRef](#)]
19. Lam, L. Design-oriented stress-strain model for FRP-confined concrete in rectangular columns. *J. Reinf. Plast. Compos.* **2003**, *22*, 1149–1186. [[CrossRef](#)]
20. Teng, J.G.; Lam, L. Behavior and modeling of fiber reinforced polymer-confined concrete. *J. Struct. Eng. ASCE* **2004**, *130*, 1713–1723.
21. Saadatmanesh, H.; Ehsani, M.R.; Li, M.W. Strength and ductility of concrete columns externally reinforced with fiber composite straps. *Struct. J.* **1994**, *91*, 434–447.
22. Chastre, C.; Silva, M.A.G. Monotonic axial behavior and modeling of RC circular columns confined with CFRP. *Eng. Struct.* **2010**, *32*, 2268–2277.
23. Wu, Y.F.; Wei, Y. General stress-strain model for steel and FRP-confined concrete. *J. Compos. Constr.* **2014**, *19*, 04014069. [[CrossRef](#)]
24. Ahmad, M.S.; Adnan, S.M.; Zaidi, S.; Bhargava, P. A novel support vector regression (SVR) model for the prediction of splice strength of the unconfined beam specimens. *Constr. Build. Mater.* **2020**, *248*, 118475. [[CrossRef](#)]
25. Duan, Z.H.; Kou, S.C.; Poon, C.S. Using artificial neural networks for predicting the elastic modulus of recycled aggregate concrete. *Constr. Build. Mater.* **2013**, *44*, 524–532. [[CrossRef](#)]
26. Gian, P.L.; Andrea, P.; Gaetano, M. Simplified modeling of rectangular concrete Cross-Sections confined by external FRP wrapping. *Polymers* **2014**, *4*, 1187–1206.
27. Boumaaza, M.; Belaadi, A.; Bouchak, M.; Jawaid, M.; Hamid, S. Comparative study of flexural properties prediction of *Washingtonia filifera* rachis biochar bio-mortar by ANN and RSM models. *Constr. Build. Mater.* **2022**, *318*, 125985.
28. Gian, P.L.; Fabio, N.; Andrea, P.; Gaetano, M. Analytical model for the effective strain in FRP-wrapped circular RC columns. *Compos. Part B* **2012**, *43*, 3209–3218.
29. Jiang, C.; Wu, Y.F. Axial strength of eccentrically loaded FRP-confined short concrete columns. *Polymers* **2020**, *5*, 1261. [[CrossRef](#)]
30. He, C.B.; Zeng, J.J. Fiber-reinforced polymer-confined non-circular columns with shape modification: A comprehensive review. *Polymers* **2022**, *14*, 564. [[CrossRef](#)] [[PubMed](#)]
31. Sharifi, Y.; Moghbeli, A. New empirical approaches for compressive strength assessment of CFRP confined rectangular concrete columns. *Compos. Struct.* **2021**, *262*, 113373. [[CrossRef](#)]
32. Ngo, N.T.; Le, H.A.; Nguyen, Q.T. Axial strength prediction of steel tube confined concrete columns using a hybrid machine learning model. In *Structures*; Elsevier: Amsterdam, The Netherlands, 2022; Volume 36, pp. 765–780.

33. Ma, L.; Zhou, C.; Lee, D.; Zhang, J. Prediction of axial compressive capacity of CFRP-confined concrete-filled steel tubular short columns based on XGBoost algorithm. *Eng. Struct.* **2022**, *260*, 114239. [[CrossRef](#)]
34. Bardhan, A.; Biswas, R.; Kardani, N.; Iqbal, M.; Samui, P.; Singh, M.P.; Asteris, P.G. A novel integrated approach of augmented grey wolf optimizer and ann for estimating axial load carrying-capacity of concrete-filled steel tube columns. *Constr. Build. Mater.* **2022**, *337*, 127454. [[CrossRef](#)]
35. Feng, D.C.; Liu, Z.T.; Wang, X.D.; Jiang, Z.M.; Liang, S.X. Failure mode classification and bearing capacity prediction for reinforced concrete columns based on ensemble machine learning algorithm. *Adv. Eng. Inform.* **2020**, *45*, 101126. [[CrossRef](#)]
36. Baietti, G.; Shahreza, S.K.; Santandrea, M.; Carloni, C. Concrete columns confined with SRP: Effect of the size, cross-sectional shape and amount of confinement. *Constr. Build. Mater.* **2021**, *275*, 121618. [[CrossRef](#)]
37. Al Abadi, H.; Paton-Cole, V.; Patel, V.I.; Thai, H.T. Axial strength and elastic stiffness behaviour of partially confined concrete columns. *Constr. Build. Mater.* **2019**, *196*, 727–741. [[CrossRef](#)]
38. Wang, Z.; Xie, J.; Jiang, X.F.; Yan, J.B. Behaviours of reinforced concrete-filled GFRP tube stub columns under low-temperature axial compression. *Constr. Build. Mater.* **2021**, *312*, 125429. [[CrossRef](#)]
39. Amiri, M.; Hatami, F. Prediction of mechanical and durability characteristics of concrete including slag and recycled aggregate concrete with artificial neural networks (ANNs). *Constr. Build. Mater.* **2022**, *325*, 126839. [[CrossRef](#)]
40. Jayasinghe, T.; Gunawardena, T.; Mendis, P. Assessment of shear strengths of reinforced concrete beams without shear reinforcement: A comparative study between codes of practice and artificial neural network. *Case Stud. Constr. Mater.* **2022**, *16*, e01102. [[CrossRef](#)]
41. Vapnik, V.N. *The Nature of Statistical Learning Theory*; Springer: New York, NY, USA, 1995.
42. Tran, V.Q.; Dang, V.Q.; Ho, L.S. Evaluating compressive strength of concrete made with recycled concrete aggregates using machine learning approach. *Constr. Build. Mater.* **2022**, *323*, 126578. [[CrossRef](#)]
43. Pessiki, S.; Harries, K.A.; Kestner, J.T.; Sause, R.; Ricles, J.M. Axial behavior of reinforced concrete columns confined with FRP jackets. *J. Compos. Constr.* **2001**, *5*, 237–245. [[CrossRef](#)]
44. Aire, C.; Gettu, R.; Casas, J.R. Study of the compressive behavior of concrete confined by fiber reinforced composites. *Carbon* **2001**, *1*, 239–243.
45. Liang, M. *Study on Strength and Deformation Characteristics of CFRP Confined Concrete Cylinder*; Dalian University of Technology: Dalian, China, 2012. (In Chinese)
46. Irandegani, M.A.; Zhang, D.; Shadabfar, M. Probabilistic assessment of axial load-carrying capacity of FRCM-strengthened concrete columns using artificial neural network and Monte Carlo simulation. *Case Stud. Constr. Mater.* **2022**, e01248. [[CrossRef](#)]
47. Liu, Z.; Sextos, A.; Guo, A.; Zhao, W. ANN-based rapid seismic fragility analysis for multi-span concrete bridges. In *Structures*; Elsevier: Amsterdam, The Netherlands, 2022; Volume 41, pp. 804–817.
48. Ghorbani, B.; Arulrajah, A.; Narsilio, G.; Horpibulsuk, S. Experimental investigation and modelling the deformation properties of demolition wastes subjected to freeze–thaw cycles using ANN and SVR. *Constr. Build. Mater.* **2020**, *258*, 119688. [[CrossRef](#)]
49. Huang, Y.; Zhang, J.; Ann, F.T.; Ma, G. Intelligent mixture design of steel fibre reinforced concrete using a support vector regression and firefly algorithm based multi-objective optimization model. *Constr. Build. Mater.* **2020**, *260*, 120457. [[CrossRef](#)]
50. Ahmed, F.B.; Mitu, S.M.; Biswas, R.K.; Ahsan, K.A.; Mim, S.M.; Ahmed, S. Forecast flexural strength of pervious concrete by SVR. *Mater. Today Proc.* **2021**, *45*, 5277–5284. [[CrossRef](#)]
51. Zhong, J.P.; Huo, J.S.; Li, Z. Experimental study on axial compression performance of concrete cylinder confined with CFRP at high temperature. *Highw. Eng.* **2020**, *45*. (In Chinese) [[CrossRef](#)]
52. Touhari, M.; Mitiche-Kettab, R. Behavior of FRP confined concrete cylinders: Experimental investigation and strength model. *Period. Polytech. Civ. Eng.* **2016**, *60*, 647–660. (In Chinese) [[CrossRef](#)]
53. Gao, C. *Study on Compressive Properties of FRP Confined Nanomaterial Modified Concrete Containing Recycled Brick Aggregate*; University of Hunan: Changsha, China, 2019. (In Chinese)
54. Zeng, L. *Study on Mechanical Properties of FRP Confined Recycled Concrete inner Hollow Composite Cylinder*; Guangdong University of Technology: Guangzhou, China, 2018. (In Chinese)
55. Lam, L.; Teng, J.G. Ultimate condition of fiber reinforced polymer-confined concrete. *J. Compos. Constr.* **2004**, *8*, 539–548. [[CrossRef](#)]
56. Vincent, T.; Ozbakkaloglu, T. Influence of concrete strength and confinement method on axial compressive behavior of FRP confined high- and ultra high-strength concrete. *Compos. Part B Eng.* **2013**, *50*, 413–428. [[CrossRef](#)]
57. Liu, P.C. *Study on Compression Performance and Size Effect of CFRP Confined Marine Sand Concrete Cylindrical Shaft*; Guangdong University of Technology: Guangzhou, China, 2018. (In Chinese)
58. Hu, Z.J. *Mechanical Behavior of CFRP-Confined Concrete Columns under Axial Compression*; University of Jilin: Changchun, China, 2010. (In Chinese)
59. Behnood, A.; Golafshani, E.M. Machine learning study of the mechanical properties of concretes containing waste foundry sand. *Constr. Build. Mater.* **2020**, *243*, 118152. [[CrossRef](#)]
60. Dent AJ, S.; Bisby, L.A. Comparison of confinement models for fiber-reinforced polymer-wrapped concrete. *ACI Struct. J.* **2005**, *102*, 62–72.
61. Wu, G.; Lv, Z.T. Study on stress-strain relationship of FRP confined concrete cylinder without softening section. *J. Build. Struct.* **2003**, *5*, 1–9. (In Chinese)

62. Youssef, M.N.; Feng, M.Q.; Mosallam, A.S. Stress–strain model for concrete confined by FRP composites. *Compos. Part B Eng.* **2007**, *38*, 614–628. [[CrossRef](#)]
63. Nanni, A.; Norris, M.S. FRP jacketed concrete under flexure and combined flexure-compression. *Constr. Build. Mater.* **1995**, *9*, 273–281. [[CrossRef](#)]
64. Samaan, M.; Mirmiran, A.; Shahawy, M. Model of concrete confined by fiber composites. *J. Struct. Eng.* **1998**, *124*, 1025–1031. [[CrossRef](#)]
65. Lam, L.; Teng, J.G. Strength models for fiber-reinforced plastic-confined concrete. *J. Struct. Eng.* **2002**, *128*, 612–623. [[CrossRef](#)]
66. ACI 440.2R-02. *Guide for the Design and Construction of Externally Bonded FRP Systems for Strengthening Concrete Structures*; American Concrete Institute: Indianapolis, IN, USA, 2002.
67. Ghorbani, B.; Arulrajah, A.; Narsilio, G.; Horpibulsuk, S. Experimental and ANN analysis of temperature effects on the permanent deformation properties of demolition wastes. *Transp. Geotech.* **2020**, *24*, 100365. [[CrossRef](#)]
68. Perlovsky, L.I. *Neural Networks and Intellect: Using Model-Based Concepts*; Oxford University Press: New York, NY, USA, 2001.
69. Haykin, S.; Lippmann, R. Neural networks, a comprehensive foundation. *Int. J. Neural Syst.* **1994**, *5*, 363–364.
70. Boser, B.E.; Guyon, I.M.; Vapnik, V.N. A training algorithm for optimal margin classifiers. In Proceedings of the Fifth Annual Workshop on Computational Learning Theory, Pittsburgh, PA, USA, 27–29 July 1992.
71. Smola, A.J. Regression Estimation with Support Vector Learning Machines. Master’s Thesis, Technische Universität München, Munich, Germany, 1996.
72. Li, L.; Zheng, W.Z.; Wang, Y. Prediction of moment redistribution in statically indeterminate reinforced concrete structures using artificial neural network and support vector regression. *Appl. Sci.* **2018**, *9*, 28. [[CrossRef](#)]
73. Hadi MN, S.; Li, J. External reinforcement of high strength concrete columns. *Compos. Struct.* **2003**, *65*, 279–287. [[CrossRef](#)]
74. Matthys, S.; Toutanji, H.; Taerwe, L. Stress-strain behavior of large-scale circular columns confined with FRP composites. *Struct. Eng.* **2006**, *132*, 123–133. [[CrossRef](#)]
75. Sadeghian, P.; Rahai, A.R.; Ehsani, M.R. Experimental study of rectangular RC columns strengthened with CFRP composites under eccentric loading. *J. Compos. Constr.* **2010**, *14*, 443–450. [[CrossRef](#)]
76. Wang, L.M.; Wu, Y.F. Effect of corner radius on the performance of CFRP-confined square concrete columns: Test. *Eng. Struct.* **2007**, *30*, 493–505. [[CrossRef](#)]
77. Mirmiran, A.; Shahawy, M.; Beitleman, T. Slenderness limit for hybrid FRP-concrete columns. *J. Compos. Constr.* **2001**, *5*, 26–34. [[CrossRef](#)]
78. Saafi, M.; Toutanji, H.; Li, Z.J. Behavior of concrete columns confined with fiber reinforced polymer tubes. *ACI Struct. J.* **1999**, *96*, 500–509.
79. Toutanji, H.; Deng, Y. Strength and durability performance of concrete axially loaded members confined with AFRP composite sheets. *Compos. Part B* **2002**, *33*, 255–261. [[CrossRef](#)]
80. Watanabe, K.; Nakamura, R.; Honda, Y.; Toyoshima, M.; Fujimaki, T. Confinement effect of FRP sheet on strength and ductility of concrete cylinders under uniaxial compression. In Proceedings of the Third International Symposium on Non-Metallic Reinforcement for Concrete Structures, Sapporo, Japan, 14–16 October 1997.
81. Lim, J.C.; Ozbakkloglu, T. Factors influencing hoop rupture strains of FRP-confined concrete. *Appl. Mech. Mater.* **2014**, *501*, 949–953. [[CrossRef](#)]
82. Almusallam, T.H. Behavior of normal and high-strength concrete cylinders confined with E-glass/epoxy composite laminates. *Compos. Part B* **2006**, *38*, 629–639. [[CrossRef](#)]
83. Berthet, J.F.; Ferrier, E.; Hamelin, P. Compressive behavior of concrete externally confined by composite jackets: Part A: Experimental study. *J. Constr. Build. Mater.* **2005**, *19*, 223–232. [[CrossRef](#)]
84. Chaallal, O.; Shahawy, M.; Hassan, M. Performance of axially loaded short rectangular columns strengthened with carbon fiber-reinforced polymer wrapping. *J. Compos. Constr.* **2003**, *7*, 200–208. [[CrossRef](#)]